ChemComm

COMMUNICATION

View Article Online
View Journal | View Issue

Cite this: *Chem. Commun.*, 2025, 61, 3335

Received 9th December 2024,
Accepted 21st January 2025

DOI: 10.1039/d4cc06481j

rsc.li/chemcomm

Pyrococcus furiosus Argonaute-mediated dual recognition enables the detection of trace single-nucleotide-mutated fungicide-resistant fungal pathogens†

Jiahao Lin,‡[abc] Jiannan Zhang,‡[d] Xianglin Zhu,[c] Xuhan Xia,[c] Yong Zhang,[c] Qingdong Zeng,[f] Yuanhong Xu,[a] Ruijie Deng *[c] and Jinghong Li *[be]

Detection of low-abundance mutations for the early discovery of fungicide-resistant fungal pathogens is highly demanded, but remains challenging. Herein, we developed a dual-recognition strategy, termed PARPA, involving *Pyrococcus furiosus* Argonaute (pfAgo)-mediated elimination of wild-type fungal genes and CRISPR/Cas12a-based amplicon recognition. This assay can detect fungicide-resistant *Puccinia striiformis* at relative abundances as low as 0.05% and has potential for achieving early screening of fungicide-resistant fungal pathogens.

Crop fungal diseases during epiphytotic years cause limited yield and economic losses globally, posing a substantial threat to food security.[1,2] Stripe rust, arising from *Puccinia striiformis* (*Pst*), is one of the most severe such fungal diseases; it causes crop yield losses exceeding 50% and destroys the whole crop in extreme cases.[3–5] To prevent fungal diseases, several efficient fungicide reagents have been developed and extensively applied. However, the improper use of fungicides has accelerated the evolution of fungicide-resistant crop-destroying fungi, causing long-term yield losses of about 20% and a 10% postharvest loss worldwide. This situation also undermines the efficacy of disease control measures.[6,7] In recent years, substantial research has uncovered resistance mechanisms,[8–10] revealing that single-nucleotide mutations (SNMs) on vital enzymes of biochemical pathways play a key role in the development of fungicide resistance.[11–13] For example, a SNM involving a mutation of A to T at position 401 in the gene that encodes the cytochrome P450 sterol 14a-demethylase enzyme (CYP51) leads to an amino acid residue change (Y134F), endowing *Pst* with resistance to triadimefon.[13] Early screening of fungicide-resistant pathogens *via* detecting SNMs in critical fungal genes is effective at hindering the spread of these pathogens and can facilitate the precise monitoring and management of crop fungal diseases.

Current strategies for detecting crop fungal infection, such as microscopic examination and antibody-based methods, are widely applied but cannot recognize genetic changes and have limited sensitivity.[14–17] While antibody-based methods, such as lateral flow assays, have been commercialized and widely used, detections based on antigen recognition results show low sensitivity, are susceptible to false-positive results, and are unable to identify genetic information changes, such as SNMs.[18–22] Nucleic acid (NA)-based methods, in contrast, show promise at detecting subtle changes in genetic information. Direct analysis of SMNs involves the DNA sequencing technique, but traditional sequencing technology typically requires a mutation allele frequency of at least 1–5% to reliably detect mutations.[23,24] While high-throughput sequencing can increase sensitivity, it is costly, operationally complex and time consuming.[25,26] These issues pose challenges for rapid point-of-care diagnosis. The polymerase chain reaction (PCR) is a time-saving approach, but it relies on a thermal cycling device, thus restricting the application for on-site detection.[27,28] The development of isothermal nucleic acid amplification methods has circumvented the limitations resulting from having to carry out a thermal cycling process.[29–31] Of these methods, recombinase polymerase amplification (RPA) is an efficient strategy due to its mild reaction conditions, simple design of primers used, and high degree of commercialization.[30,31] However, it remains challenging to use RPA-based techniques to detect SNMs in pathogenic genes due to the difficulty in applying RPA primers to discriminate SNMs.

[a] *Institute of Biomedical Engineering, College of Life Sciences, Qingdao University, Qingdao 266071, China*
[b] *Beijing Life Science Academy, Beijing 102206, China*
[c] *College of Biomass Science and Engineering, Sichuan University, Chengdu 610065, China. E-mail: drj17@scu.edu.cn*
[d] *Key Laboratory of Bio-resources and Eco-environment of Ministry of Education, College of Life Sciences, Sichuan University, Chengdu 610065, China*
[e] *Department of Chemistry, Center for BioAnalytical Chemistry, Key Laboratory of Bioorganic Phosphorus Chemistry & Chemical Biology, New Cornerstone Science Laboratory, Tsinghua University, Beijing 100084, China*
[f] *State Key Laboratory of Crop Stress Biology for Arid Areas, Northwest A&F University, Yangling 712100, China*

† Electronic supplementary information (ESI) available: Experimental section, The expression and purification of PfAgo, optimization of RPA primers and PfAgo/crRNA ratios. See DOI: https://doi.org/10.1039/d4cc06481j

‡ These authors contributed equally to this work.

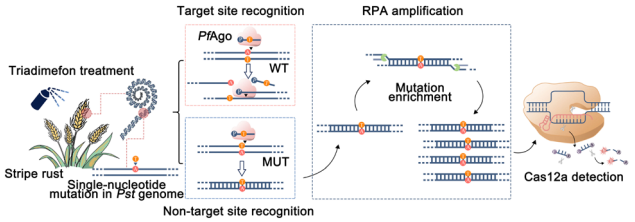

Fig. 1 Schematic illustration of the PARPA assay and its application for detecting triadimefon-resistant *Puccinia striiformis* having single-nucleotide mutations.

Herein, we propose an assay utilizing *Pyrococcus furiosus* Argonaute (*pf*Ago) coupled with RPA, termed PARPA, and CRISPR/Cas12a for specific target enrichment and detection, leading to the discrimination of low-abundance SNMs in the fungal gene (Fig. 1). *Pf*Ago can identify SNMs due to its ability to cleave the target sequence through complete nucleotides pairing between positions 10 and 11 of the guide single-stranded DNA (ssDNA). Hence, a mismatch of a single nucleotide near these positions can significantly affect the cleavage activity of *Pf*Ago. We utilized *Pf*Ago to recognize SNMs, employed RPA for signal amplification, and used CRISRR/Cas12a to identify the amplicons—with the dual recognition by *Pf*Ago and CRISPR/Cas12a ensuring high specificity for SNM determination, and the coupling with RPA guaranteeing a high sensitivity for fungus detection. The PARPA assay was applied to on-site diagnosis of the infection of low-abundance (0.05%) triadimefon-resistant *Pst* in wheat, and could hence benefit crop early diagnostics and management.

Based on the recognition mechanism of *Pf*Ago, a 16-nt single-stranded 5′-phosphorylated DNA with an introduced nucleotide mismatching the target gene sequence at the proper position was leveraged as a gDNA of *Pf*Ago. The WT *cyp51* gene, which is completely complementary to gDNA, triggers the cleavage activity of *Pf*Ago, leading to the removal of the WT sequence. In contrast, the MUT *cyp51* gene is protected from being cleaved due to the mismatched nucleotide within the gDNA (Fig. 2A).[32–36] After the enrichment of the MUT *cyp51* gene *via* the RPA reaction, Cas12a was introduced to recognize the target amplicons under the guidance of crRNA. Activating Cas12a to carry out *trans*-cleavage would cut off the fluorophore and quencher-modified DNA sequence that serve as the reporter, yielding a fluorescence to indicate the presence of the MUT *cyp51* gene.

SDS-PAGE was performed to confirm the identity of the purified *Pf*Ago. An expected band of *Pf*Ago at about 87 kD was found in the elution buffer, indicating that the protein of interest had been successfully expressed and collected (Fig. S1, ESI†). Electrophoresis and fluorescence analyses were performed to investigate the working principle of the PARPA assay (Fig. 2). The *cyp51* gene of *Pst* with a SNM at position 401 (A to T) was chosen as the target gene. We first optimized the primers of the RPA reaction (Fig. S2, ESI†). Then, the endonuclease activity of *Pf*Ago on the SNM site was proved using gel electrophoresis (Fig. 2B). When reacting together *Pf*Ago, gDNA, and RPA reagents, no amplicon band at 251 bp was observed in the sample containing the WT *cyp51* gene, but this band did appear in the sample containing the MUT *cyp51* gene.

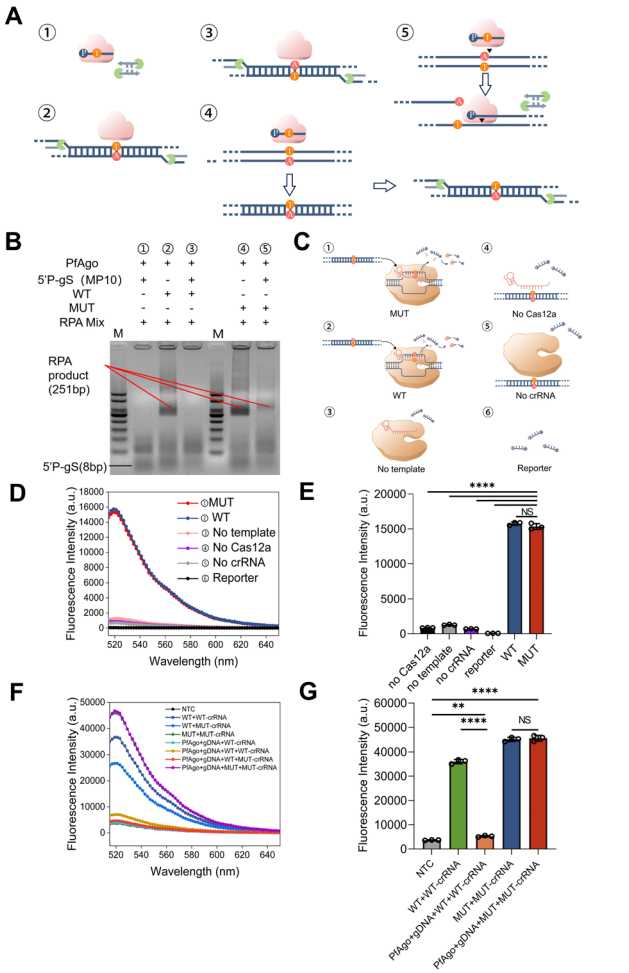

Fig. 2 Validation of the working principle of the PARPA assay. (A) Schematic illustration of the samples subjected to electrophoresis analysis. (B) Electrophoresis analysis for the investigation of the working principle. M: DNA marker (50–500 bp); 5′P-gS: a single-stranded 5′-phosphorylated gDNA; 5′P-gS (MP10): 5′P-gS with an introduced mismatched nucleotide to the target gene at the tenth position. (C) Schematic illustration of the samples subjected to fluorescence analysis. (D) Fluorescence intensities of the CRISPR/Cas12a system response to MUT or WT templates. The concentrations of Cas12a, crRNA, and reporter were 100 nM, 200 nM, and 500 nM, respectively. (E) Statistical analysis of the fluorescence intensities in Fig. 2D. (F) Fluorescence intensity of the samples used in the PARPA assay. The concentrations of *Pf*Ago, gDNA, and MUT/WT templates were 15 nM, 150 nM, and 150 fM. (G) Plot showing the ability of the PARPA assay to discriminate the MUT and WT templates. Two-tailed unpaired Student's *t*-test was carried out: $^{**}P < 0.0001$, $^{****}P < 0.0001$, NS: $P > 0.05$.

Next, we performed a fluorescence test to verify the *trans*-cleavage activity of Cas12a with regards to the reporter (Fig. 2C). As illustrated in Fig. 2D and E, the fluorescence intensities of the WT and the MUT amplicons rapidly increased about 12 fold from that of the negative control to values of 15 737 and 15 319 when mixing together Cas12a and the reporters with, respectively, WT-crRNA and MUT-crRNA. The dramatic enhancement in fluorescence intensity indicated that the *trans*-cleavage ability of Cas12a was activated as the Cas12a/crRNA complex specifically recognized the amplicons of RPA. Finally, a fluorescence analysis was conducted to further verify the feasibility of

deploying the PARPA assay for SNM detection (Fig. 2F). The tested sample of WT *cyp51* exhibited a low fluorescence intensity when treated with *Pf*Ago and relevant gDNA, while the fluorescence intensities of the MUT *cyp51* sample and *Pf*Ago/gDNA complex remained as high as that of the sample not subjected to *Pf*Ago/gDNA treatment (Fig. 2G). These results indicated that the PARPA assay can not only precisely discriminate a single nucleotide difference between the WT gene and the MUT gene under the guidance of a guide DNA but also successfully enrich the target MUT gene and yield a high fluorescence after RPA reaction and Cas12a recognition.

Due to a high specificity of the PARPA assay, relying on the precise recognition of SNMs by the *Pf*Ago/gDNA complex, the position of mismatched nucleotides in gDNA needed to be optimized. The gDNAs for *Pf*Ago were designed as short 16-nt ssDNAs with introduced mismatched nucleotides at different positions (Table S1, ESI†). We tested the effectiveness of these gDNAs with different positions for the mismatching by assessing the cleavage activity of Cas12a towards reporter with the addition of the WT and MUT genes. The ratio of fluorescence intensities using the MUT and WT genes (MUT/WT) was applied to assess the discrimination capacity of SNMs. The *Pf*Ago/gDNA complex showed the best SNM discrimination performance when the single nucleotide mismatch was introduced into the tenth position of the gDNA (producing a guide DNA denoted as gS(MP10)), the MUT/WT ratio was 5.7 (Fig. S3A, ESI†). This result coincided with the substrate binding mode for *Pf*Ago proposed in previous reports, in which the scissile bond was found to be between nucleotides 10 and 11 from the 5′ end of the guide.[37,38] This mode induced the PIWI domain of *Pf*Ago to recognize and cleave the target site.[37–41]

After the optimization of the *Pf*Ago/gDNA complex for SNM discrimination, we investigated the performance of CRISPR/Cas12a. The targeting site of crRNA is a key factor in determining the effectiveness of Cas12a. The crRNAs were designed according to protospacer adjacent motif (PAM, 5′-TTN-3′) recognition sites around the SNMs and a mismatched nucleotide was introduced at the site complementary to the target SNMs to enhance the SNM discrimination (Fig. S3B, ESI†). Then, the fluorescence changes resulting from CRISPR/Cas12a system cleaving the reporter was used to assess the performance of designed crRNAs. A maximum MUT/WT ratio of 3.44 was found when the MUT-crRNA3 was employed (Fig. S3C, ESI†). In addition, the PAM site preference of crRNA3 was further investigated. The CRISPR/Cas12a system effectively identified the target sequence only when the crRNA3 was designed to be near the specific PAM site of Cas12a (TTN, N = A, T, C, or G) (Fig. S3D, ESI†). The results proved the selected MUT-crRNA3 to be highly specific for the mutant sequence.

Non-specific cleavage may occur for a concentration of gDNA lower than that of *pf*Ago, and can affect the efficiency of SNM discrimination.[32–36,41,42] Hence, we investigated the effect of the ratio of *Pf*Ago to gDNA on SNM detection (Fig. S4, ESI†). Samples of gDNA at a concentration of 150 nM were, respectively, incubated with *Pf*Ago samples of different concentrations (15 μM, 15 nM, and 15 pM) and then each tested for their abilities to recognize 15 fM of the WT or MUT *Pst* template. When the *Pf*Ago to gDNA ratio was 1 : 10, the fluorescence intensity of the MUT template was 5.28-fold higher than that of the WT template, and was the best-performing ratio for SNM discrimination. In general, to optimally distinguish target, appropriate ratios of *Pf*Ago to gDNA are required to effectively cut the WT gene and avoid undesired cutting of the MUT gene.[32–36] In the proposed assay, 1 : 10 was chosen as the optimal ratio of *Pf*Ago to gDNA for detecting SNMs.

We investigated the capacity of the PARPA assay for detecting the MUT *cyp51* gene using the optimized gDNA and crRNA (Fig. S5, ESI†). The MUT and WT gene fragments were prepared by performing PCR from plasmids carrying MUT and WT genes of *cyp51*. Then, the samples for testing were prepared by mixing the WT template with the MUT template at various ratios, with the MUT *cyp51* gene making up 0.05, 0.1, 1, 10, 20, 40, and 100% of the total, respectively. The fluorescence intensity rose gradually with increasing relative amount of the MUT template (Fig. S5A and B, ESI†). This result indicated that the PARPA assay enabled the detection of the SNM at a relative amount as low as 0.05%. In contrast, the CRISPR-based RPA method without the *pf*Ago enrichment could only detect the SNM at a higher relative amount of 1% (Fig. S5C and D, ESI†), which is similar to the results for those methods using sequencing[23,24] and ARMS-PCR.[43,44] Hence, the proposed dual recognition using *Pf*Ago and CRISPR-Cas12a yielded a 20-fold increase in the sensitivity of SNM recognition. We further evaluated the capability of PARPA to detect 0.05% single-nucleotide mutations across DNA concentrations ranging from 20 fM to 20 nM. It was found to maintain remarkable sensitivity in samples at concentrations as low as 20 pM (Fig. S6, ESI†). These results proved the PARPA assay to be one of the most sensitive methods for detecting trace SNMs (Table S3, ESI†).

The performance of the PARPA assay for the detection of triadimefon-resistant *Pst* was further estimated. First, three *P. striiformis* isolates, termed *Pst*-A, *Pst*-B, and *Pst*-C, respectively, were collected from Sichuan province, China. We then tested these isolates using the PARPA assay. *Pst*-A and *Pst*-B yielded fluorescence values of up to 13 256 and 12 572 respectively, which were much higher than those of *Pst*-C and the negative control (Fig. 3A). This result indicated the possibility of the Y134F mutation being present in the genomes of *Pst*-A and *Pst*-B. To confirm the occurrence of a mutation from A to T at position 401 in these cases, genome sequencing was conducted, and verified the presence of the SNM. Different proportions of the A to T mutation were identified in the gene sequences of *Pst*-A and *Pst*-B (42.4% and 45%, respectively). In contrast, no SNM was observed in the genome of *Pst-C* (Fig. 3B).

The stripe rust phenotypes of wheat leaves inoculated with *Pst*-A, *Pst*-B and *Pst*-C were assessed. Values of half-maximal effective concentration (EC_{50}) of triadimefon (one of demethylation inhibitor fungicides) working on the three *Pst* isolates were determined to evaluate the triadimefon sensitivities of the three isolates. The EC50 values of triadimefon for *Pst*-A, *Pst*-B and *Pst*-C were 2.15, 1.62, and 0.12 mg L^{-1}, respectively, indicating that *Pst*-A and *Pst*-B were triadimefon-resistant

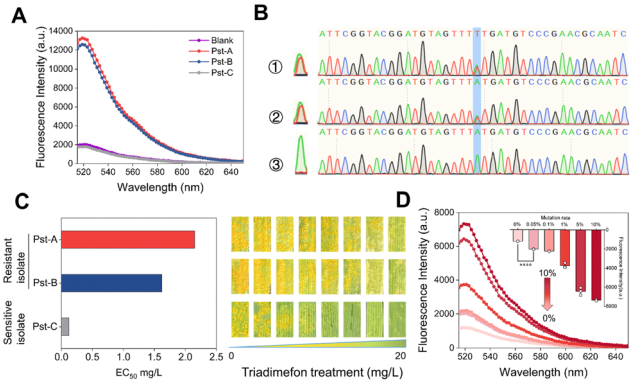

Fig. 3 Detection performance of the PARPA assay for identifying triadimefon-resistant *Pst* and triadimefon-sensitive *Pst*. (A) Fluorescence intensities of three *Pst* isolates using the PARPA assay. (B) Sequencing results for the *cyp51* gene in the three *Pst* isolates. (C) Plot of values of EC_{50} of triadimefon tested on the *Pst* isolates, and images showing stripe rust phenotypes of samples of wheat leaves each inoculated with a different *Pst* isolate. (D) Fluorescence analysis of the PARPA assay responses to different proportions of triadimefon-resistant *Pst* isolates. Two-tailed unpaired Student's *t*-test was carried out: ****$P < 0.0001$.

strains and *Pst*-C was a triadimefon-sensitive strain (Fig. 3C). These results corresponded with the results shown in Fig. 3A and B and proved that the PARPA assay can precisely identify the SNM of *Pst*. Furthermore, the PARPA assay performance at enriching and detecting low-abundance mutated alleles in complex samples was estimated. We investigated the PARPA assay capacity at discriminating rare mutated alleles from the abundant WT gene using 20 pM samples that were prepared by mixing *Pst*-C with *Pst*-B in various proportions (Fig. 3D). The fluorescence intensity increased gradually as the proportion of *Pst*-B increased from 0 to 10%. The lowest detectable proportion of *Pst*-B was 0.05%. In comparison to the 1–5% detection limits for SNMs in sequencing,[23–26] the PARPA assay yielded a higher sensitivity in detection of low-abundance mutant alleles.

In summary, we have developed a PARPA assay for highly sensitive detection of single-nucleotide-mutated fungicide-resistant fungus *via* a dual-recognition strategy. The dual-recognition process involving *Pf*Ago and CRISPR/Cas12 endowed the PARPA assay with high specificity to detect low-abundance SNMs. The amplification process combining RPA and CRISPR/Cas12 provided a high sensitivity to detect the SNM-containing gene. These features allowed the PARPA assay to detect *Pst*, one of the main pathogens threatening crop yield, and discriminated trace SNMs with only 0.05% abundance in a mixture of *Pst* strains. Furthermore, the strict temperature control process was eliminated using RPA, thus facilitating on-site detection. The PARPA assay enables the early identification of fungicide-resistant phenotypes in pathogens during the initial stages of crop disease, providing a valuable tool for enhancing the precision of plant disease control and management.

The work is supported by National Natural Science Foundation of China (No. 22027807, No. 22074100), the National Key Research and Development Program of China (No. 2021YFA1200104), the New Cornerstone Investigator Program.

Data availability

The data underlying this study are available in the published article and its ESI.†

Conflicts of interest

The authors have declared no conflict of interest.

Notes and references

1 M. C. Fisher, *et al.*, *Nature*, 2012, **484**, 186–194.
2 J. C. M. Villamil, *et al.*, *Nat. Commun.*, 2019, **10**, 15.
3 V. Klymiuk, *et al.*, *Nat. Commun.*, 2018, **9**, 12.
4 X. M. Chen, *Food Secur.*, 2020, **12**, 239–251.
5 N. Wang, *et al.*, *Cell*, 2022, **185**, 2961–2974.
6 M. C. Fisher, *et al.*, *Science*, 2018, **360**, 739–742.
7 J. H. Wu, *et al.*, *Plant Dis.*, 2020, **104**, 1751–1762.
8 Z. H. Ma and T. J. Michailides, *Crop Prot.*, 2005, **24**, 853–863.
9 N. J. Hawkins and B. A. Fraaije, *Annu. Rev. Phytopathol.*, 2018, **56**, 339–360.
10 M. J. Hu and S. N. Chen, *Microorganisms*, 2021, **9**, 19.
11 H. F. Avenot and T. J. Michailides, *Crop Prot.*, 2010, **29**, 643–651.
12 Y. Tian, *et al.*, *Front. Microbiol.*, 2019, **10**, 11.
13 N. M. Cook, *et al.*, *Pest Manag. Sci.*, 2021, **77**, 3358–3371.
14 H. Y. Lau and J. R. Botella, *Front. Plant Sci.*, 2017, **8**, 14.
15 A. Suea-Ngam, *et al.*, *ACS Sens.*, 2020, **5**, 2701–2723.
16 R. Patel, *et al.*, *Talanta*, 2023, **251**, 9.
17 K. Da Cunha and L. Fontao, *J. Med. Mycol.*, 2016, **26**, 22–23.
18 J. Yu, *et al.*, *Lett. Appl. Microbiol.*, 2019, **69**, 64–70.
19 W. J. Qian, *et al.*, *J. Agr. Food Chem.*, 2018, **66**, 5473–5480.
20 T. Wang, *et al.*, *Sci. Rep.*, 2017, **7**, 4348.
21 A. Silva, *et al.*, *J. Clin. Microbiol.*, 2020, **58**, 12.
22 Y. F. Pang, *et al.*, *Chem. Eng. J.*, 2022, **429**, 13219.
23 A. M. Newman, *et al.*, *Nat. Med.*, 2014, **20**, 552–558.
24 C. Callens, *et al.*, *Anal. Chem.*, 2022, **94**, 6297–6303.
25 L. R. Wu, *et al.*, *Nat. Biomed. Eng.*, 2017, **1**, 714–723.
26 P. Song, *et al.*, *Nat. Biomed. Eng.*, 2021, **5**, 690–701.
27 M. N. Kabir, *et al.*, *Microorganisms*, 2020, **8**, 15.
28 K. Q. Mu, *et al.*, *J. Agric. Food Chem.*, 2022, **70**, 7240–7247.
29 K. W. Hsieh, *et al.*, *Angew. Chem., Int. Ed.*, 2012, **51**, 4896–4900.
30 H. Y. Lau, *et al.*, *Anal. Chem.*, 2016, **88**, 8074–8081.
31 H. Y. Lau, *et al.*, *Sci. Rep.*, 2017, **7**, 7.
32 Q. Liu, *et al.*, *Nucleic Acids Res.*, 2021, **49**, 14.
33 F. Wang, *et al.*, *Biosens. Bioelectron.*, 2021, **177**, 6.
34 G. Xun, *et al.*, *Bioresour. Bioprocess.*, 2021, **8**, 46.
35 C. J. Zhao, *et al.*, *Anal. Chem.*, 2022, **94**, 17151–17159.
36 R. Y. He, *et al.*, *Chem. Commun.*, 2019, **55**, 13219–13222.
37 Y. L. Wang, *et al.*, *Nature*, 2008, **456**, 921–927.
38 D. C. Swarts, *et al.*, *Nucleic Acids Res.*, 2015, **43**, 5120–5129.
39 D. C. Swarts, *et al.*, *Nat. Struct. Mol. Biol.*, 2014, **21**, 743–753.
40 J. W. Hegge, *et al.*, *Nat. Rev. Microbiol.*, 2018, **16**, 5–11.
41 J. Z. Song, *et al.*, *Nucleic Acids Res.*, 2020, **48**, e19.
42 A. Kuzmenko, *et al.*, *Nucleic Acids Res.*, 2019, **47**, 5822–5836.
43 G. Ellison, *et al.*, *J. Exp. Clin. Cancer Res.*, 2010, **29**, 132.
44 H. Yang, *et al.*, *J. Agric. Food Chem.*, 2022, **70**, 8451–8457.

